Colloids and Surfaces B: Biointerfaces 167 (2018) 73–81

Contents lists available at ScienceDirect

Colloids and Surfaces B: Biointerfaces

journal homepage: www.elsevier.com/locate/colsurfb

Carbamazepine-loaded solid lipid nanoparticles and nanostructured lipid carriers: Physicochemical characterization and *in vitro*/*in vivo* evaluation

S. Scioli Montoto[a], M.L. Sbaraglini[a], A. Talevi[a], M. Couyoupetrou[b], M. Di Ianni[a], G.O. Pesce[b], V.A. Alvarez[c], L.E. Bruno-Blanch[a], G.R. Castro[d], M.E. Ruiz[a,*], G.A. Islan[d,*]

[a] *Laboratorio de Investigación y Desarrollo de Bioactivos (LIDeB), Departamento de Ciencias Biológicas, Facultad de Ciencias Exactas, Universidad Nacional de La Plata (UNLP), Calle 47 y 115, B1900AJI, La Plata, Buenos Aires, Argentina*
[b] *Departamento de Farmacología, Instituto Nacional de Medicamentos (INAME), Administración Nacional de Medicamentos, Alimentos y Tecnología Médica (ANMAT), CABA, Buenos Aires, Argentina*
[c] *Grupo de Materiales Compuestos de Matriz Polimérica (CoMP), Instituto de Investigaciones en Ciencia y Tecnología de Materiales (INTEMA), Facultad de Ingeniería, Universidad Nacional de Mar del Plata (UNMDP) – CONICET, Solis 7575, B7608FDQ, Mar del Plata, Buenos Aires, Argentina*
[d] *Laboratorio de Nanobiomateriales, CINDEFI, Departamento de Química, Facultad de Ciencias Exactas, Universidad Nacional de La Plata (UNLP) -CONICET (CCT La Plata), Calle 47 y 115, B1900AJI, La Plata, Buenos Aires, Argentina*

ARTICLE INFO

Article history:
Received 1 November 2017
Received in revised form 21 February 2018
Accepted 30 March 2018
Available online 31 March 2018

Keywords:
Carbamazepine
Solid lipid nanoparticles
Nanostructured lipid carriers
Controlled release
Refractory epilepsy
Central nervous system

ABSTRACT

Solid lipid nanoparticles (SLN) and nanostructured lipid carriers (NLC) represent promising alternatives for drug delivery to the central nervous system. In the present work, four different nanoformulations of the antiepileptic drug Carbamazepine (CBZ) were designed and prepared by the homogenization/ultrasonication method, with encapsulation efficiencies ranging from 82.8 to 93.8%. The formulations remained stable at 4 °C for at least 3 months. Physicochemical and microscopic characterization were performed by photon correlation spectroscopy (PCS), transmission electron microscopy (TEM), atomic force microscopy (AFM); thermal properties by differential scanning calorimetry (DSC), thermogravimetry (TGA) and X-ray diffraction analysis (XRD). The results indicated the presence of spherical shape nanoparticles with a mean particle diameter around 160 nm in a narrow size distribution; the entrapped CBZ displayed an amorphous state. The *in vitro* release profile of CBZ fitted into a Baker-Lonsdale model for spherical matrices and almost the 100% of the encapsulated drug was released in a controlled manner during the first 24 h. The apparent permeability of CBZ-loaded nanoparticles through a cell monolayer model was similar to that of the free drug. *In vivo* experiments in a mice model of seizure suggested protection by CBZ-NLC against seizures for at least 2 h after intraperitoneal administration. The developed CBZ-loaded lipid nanocarriers displayed optimal characteristics of size, shape and drug release and possibly represent a promising tool to improve the treatment of refractory epilepsy linked to efflux transporters upregulation.

1. Introduction

The application of nanotechnology in the field of drug delivery is a growing trend in academy and industry, driven by its many possibilities and the already achieved successes [1]. The development of pharmaceutical nanotechnology is now in a more mature age, dominated by the rational search and design of nanosystems that can offer improved drug delivery with high margins of safety [2,3].

Drug encapsulation into nanosystems can help to overcome many of the challenges commonly found in the treatment of Central Nervous System (CNS) conditions, mainly owed to the presence of the blood-brain barrier (BBB) [4,5]. This protective barrier presents not only particularly occlusive tight junctions which limit the paracellular diffusion pathway, but also high levels of expression of poly-specific efflux pumps of the ABC superfamily (*i.e.* P-gp, BCRP, MRPs), which restrict the transfer of their substrates through the transcellular pathway [6].

* Corresponding authors.
E-mail addresses: eruiz@biol.unlp.edu.ar (M.E. Ruiz), germanislan@biol.unlp.edu.ar (G.A. Islan).

https://doi.org/10.1016/j.colsurfb.2018.03.052
0927-7765/

In particular, the present work focuses on epilepsy, a brain disease characterized by the presence of recurrent and spontaneous seizures [7]. According to the World Health Organization, it is one of the more frequent neurological diseases, globally affecting near 0.4–1.0% of the population, which approximately corresponds to 50 million people [8]. The first-line treatment for epilepsy is symptomatic: seizures are inhibited by chronic administration of one or more antiepileptic drugs (AEDs). However, many patients are unable to achieve seizure control, owing to drug resistance and treatment discontinuation [9,10]. Refractory epilepsy (failure to respond to two appropriately chosen, well-tolerated AEDs) occurs in around 30% of the patients [11].

Development of new drugs is a classic approach to address the matter, but although during the last two decades numerous novel AEDs were launched, the proportion of refractory patients has remained unmodified [12,13]. While the last generation drugs possess better pharmacokinetics and/or safety profiles and provide solutions for certain specific types of epilepsy, their market prices are 10–100 fold higher than classic AEDs [14]. Bearing in mind that 80% of the people with epilepsy come from low- and middle-income countries, there is an urgent need for improved therapeutic approaches using first- and second-generation, accessible drugs [8,15].

An increased number of nanosystems have been developed and tested as potential drug delivery systems for AEDs. Briefly, synthetic polymer-based nanocarriers have been the most widely studied [16–22]. With the advantage of more control over some system properties, like particle size, surface properties and degradation kinetics, the preparation of polymeric nanoparticles (NPs) is usually complicated, with highly toxic solvents needed [23]. On the other hand, biopolymers like chitosan [24,25] or albumin [26] have also been used to prepare NPs that carry AEDs, to achieve good biocompatibility and green preparations procedures. However, these naturally occurring molecules exhibit high batch-to-batch variability, and their high water solubility leads to poor encapsulation efficiencies of lipophilic drugs [27,28]. Moreover, since they are self-assembled systems, their stability upon dilution in the physiological environment may be compromised [5], and crosslinking techniques may affect the final particle size and release kinetics [29,30].

Among the different groups of nanosystems, lipid particulate nanosystems (*i.e.* solid lipid nanoparticles, SLN; and nanostructured lipid carriers, NLC) seem to be especially suitable for drug delivery applications in brain delivery due to their inherent ability to cross the BBB [31,32]. They possess practically the same advantages of polymeric NPs, but they can be manufactured with non-toxic lipid materials without the use of organic solvents, resulting in safer and more stable biodegradable and biocompatible designs [33]. In addition, the surface of these nanocarriers can be tailored by functionalization with molecules like Apo-E, anti-Contactin-2 or anti-Neurofascin that could enhance the passage through the BBB [34,35].

With regard to AEDs, lipid-based nanosystems containing Diazepam [36], Valproate [37] and Clonazepam [38] have been explored. In all these cases the resulting nanosystems were above 200 nm of diameter *(i.e.* in a size range associated with rapid opsonization and uptake by the RES [39]), The *in vivo* results of the Clonazepam SLN showed that PK improvements did translate into a superior pharmacodynamic behaviour, since the nanoformulations enhance the protection against seizures in different preclinical models of acute epilepsy [38].

Although it is still not well established if CBZ is a substrate of efflux pumps [40], the inclusion of the drug into NPs could provide other therapeutic advantages, among the possible reduction in the conversion rate to its 10,11-epoxide derivative. Such active metabolite has sometimes been regarded as the responsible for the main toxic effects, also being a P-gp substrate with shorter half-life than the parent drug [41,42].

To our best knowledge, the only previous report of a nanocarrier for CBZ consisted on chitosan-SLN prepared by the solvent-injection method [43]. An improved *in vivo* performance in two different animal models of seizure using the chitosan-SLN-CBZ formulation was claimed by the authors, though the administered doses have not been clearly specified and some controls are missing [27].

Here we present the synthesis, characterization and *in vivo* evaluation of lipid NPs containing the first-generation AED CBZ, with the final goal of increasing the drug bioavailability at the brain parenchyma. Physicochemical characterization of the formulations was performed by photon correlation spectroscopy (PCS), transmission electron (TEM), atomic force microscopy (AFM), differential scanning calorimetry (DSC), thermogravimetry (TGA) and X-ray diffraction analysis (XRD). Stability studies have also been performed. The CBZ *in vitro* kinetic release was analysed by structured models. CBZ permeability studies were performed in Madin–Darby canine kidney transfected with MDR1 (MDCK-MDR1) epithelial cells and the *in vivo* anticonvulsant activity was studied in mice. To the best of our knowledge, this is the first report of NLC for the delivery of CBZ.

2. Materials and methods

2.1. Materials

Lipid myristyl myristate (Crodamol® MM, melting range = 36–40 °C), cetyl esters wax NF (Crodamol® SS, melting point ~44 °C), and the oil (Crodamol® GTCC-LQ, a triglyceride with saturated fatty acids, melting point = −4 °C) were kindly donated by Croda (Argentina). CBZ (98.1% as basis) was provided by Saporiti (Argentina). Kolliphor® P188 was provided by Sigma-Aldrich (Buenos Aires, Argentina). Other reagents were of HPLC/analytical grade.

2.2. Preparation of CBZ loaded SLN and NLC

CBZ-loaded SLN and NLC were prepared by melt-emulsification followed by ultrasonication technique [44,45]. Briefly, 400 mg of lipid MM or SS were melted into a water bath at 70 °C and mixed with 5 mg of CBZ, as powder or dissolved in 50 μl of dimethyl sulfoxide (DMSO). For the preparation of NLC, 12 μl of oil were added to the melted lipid phase before drug incorporation. After 30 min, 20 ml of an aqueous solution of Kolliphor® P188 (3% w/v), preheated at 70 °C, were poured over the lipid phase (2% w/v). Promptly, mixture was ultrasonicated for 50 min, at 90% amplitude using an ultrasonic processor (130 W, Cole-Parmer, USA) equipped with a 3-mm titanium tip. Once the sonication process was finished, the resulting suspension was rapidly cooled to room temperature and the remaining volume was measured.

Theoretical drug loading (DL, %) was calculated as follows:

$$DL(\%) = \frac{Mass\ of\ drug\ incorporated\ (mg)}{Lipid\ mass\ (mg)} x100 \quad (1)$$

In this way, four different formulations were obtained: two with CBZ incorporated as a powder (SLN-CBZ and NLC-CBZ) and other two formulations with the drug previously dissolved in DMSO [SLN-CBZ (DMSO) and NLC-CBZ (DMSO)].

2.3. Measurement of entrapment efficiency

Entrapment efficiency (EE, %) of all formulations was determined by measuring the concentration of the non-encapsulated

drug in solution [45]. A suitable volume (*ca.*500 μl) of the final suspension was placed in Microcon® centrifugal filters (10 kDa, Merck Millipore, Billerica, MA, USA). After centrifugation, the concentration of free CBZ was measured using a HPLC method. Considering the initial amount of CBZ added to each formulation, the EE was calculated as:

$$EE\,(\%) = \frac{W_0 - \left(C_{fr} \times V_f\right)}{W_0} \times 100 \quad (2)$$

where W_0 is the initial amount of CBZ added to the formulation, C_{fr} is the free drug concentration in μg/ml, and V_f is the final volume in ml, after ultrasonication.

2.4. HPLC analysis of CBZ

Chromatographic analysis was performed using a Dionex Ultimate 3000 UHPLC (Thermo Scientific, Sunnyvale, CA) equipped with a dual gradient tertiary pump (DGP-3000) and a DAD-3000 diode array detector. Chromatographic separation was performed in a Lichrosphere® 100 RP-18 (250 mm × 4 mm, 5 μm, Merck KGaA, Darmstadt, Germany) column. The mobile phase consisted of methanol and KH_2PO_4 buffer (70:30). The system was operated isocratically at a flow rate of 1.0 ml/min, and detection was performed at 285 nm. Samples were diluted with mobile phase and centrifuged (15,000*g* for 5 min at 4 °C) prior to their injection (20 μl).

The method was validated in terms of linearity, precision and specificity, over the range of expected concentrations. A linear correlation ($p < 0.0001$) was observed in the concentration range of 0.1–50.0 mg/L, with a coefficient of determination $r^2 = 0.997$. The 95% confidence interval of the intercept was [−1.2322–0.6447]. Precision of the method was established at three concentration levels: 0.1, 20.0 and 50.0 mg/L, and in all cases RSD values were below 3%. The method was specific for the lipid matrix and no interfering peaks were observed near CBZ retention time.

2.5. Particle size distribution, zeta potential and polydispersity index (PI)

Particle size distribution and mean diameter were measured by dynamic light scattering (DLS) using a Nano ZS Zetasizer (Malvern Instruments, Worcestershire, UK) at 25 °C in polystyrene cuvettes with a path length of 10 mm. Zeta potential was determined by Doppler anemometry using the equipment previously described. Measurements were performed in 10 mm path length capillary cells, using ultrapure water (Milli-Q®, Millipore, Ma., USA). As a dimensionless measure of the size dispersion, PI was determined. All measurements were carried out in triplicate.

2.6. Transmission electron microscopy (TEM)

TEM analysis was performed using a Jeol-1200 EX II-TEM microscope (Jeol, Columbia, MD, USA). Nanoparticles dispersions were 1:100 diluted with ultra-pure Milli-Q® water and 10 μl of each formulation was spread onto a Cu grid of 400 mesh. After incubation, the sample excess was removed with filter paper. One drop of phosphotungstic acid was added to the grid, for contrast enhancement and incubated for 1 min at 25 °C before excess removal. Finally, the grid was dried at room temperature.

2.7. Atomic force microscopy (AFM)

Milli-Q water aliquots of 1:100 dilutions of the nanoparticles dispersions were dropped on freshly cleaved mica plates, and 10 μl of Cl_2Ca (10 mM) were added. After 15 min, plates were washed with ultrapure water and excess removed with paper filter (Whatman, Germany).

All images were obtained at room temperature using a Multimode-Nanoscope V (Veeco, Santa Barbara, CA, USA) operating in tapping mode with an etched silicon probe model RTesp-Bruker (cantilever resonance frequency: 300 kHz, Force constant 42 N/m; tip radius 8–12 nm). Typical scan rates were 1 Hz.

2.8. Differential scanning calorimetry (DSC) analysis

Thermal analysis of CBZ, SLN-CBZ, SLN-CBZ (DMSO), NLC-CBZ, and NLC-CBZ (DMSO) was assessed by DSC (PerkinElmer INC., model Parys 1, Waltham, MA, USA) under nitrogen atmosphere. The heating rate was 10 °C/min in the range of 25–260 °C. A standard aluminium sample cells were used and filled with 5 mg of dry sample. Variations in the crystallinity index (CI, %) of cetyl palmitate (the main component in the wax was taken as reference) after the synthesis process were determined according to the equation proposed by Makwana et al. [46], considering the melting heat of pure stearyl stearate ($\Delta H_{CP} = 172.70\,J\,g^{-1}$) and a 2.0% lipid concentration:

$$CI\,(\%) = \frac{\Delta H_{SLN\ dispersion}\left[J.g^{-1}\right]}{\Delta H_{CP}\left[J.g^{-1}\right] \times C_{lipid\ phase}\,[\%]} \times 100 \quad (3)$$

where $\Delta H_{SLN,dispersion}$ is the melting heat of cetyl palmitate in nanoparticles, ΔH_{SS} is the melting heat of pure cetyl palmitate, and $C_{lipidphase}$ is the percentage lipid concentration within the formulation.

2.9. Thermogravimetric analysis (TGA)

To assess the thermal stability of CBZ, SLN-CBZ, SLN-CBZ (DMSO), NLC-CBZ, and NLC-CBZ (DMSO) nanoparticles, TGA was performed on a TGA Q500 apparatus (TA Instruments, New Castle, DE, USA). Samples of 6–12 mg were accurately weighed in a platinum pan and measurements conducted at a heating rate of 10 °C/min under nitrogen atmosphere.

2.10. X-ray diffraction (XRD)

The characterization of nanoparticles crystalline structure was obtained from XRD spectra data recorded in PANalytical X'Pert PRO diffractometer equipped with an X-ray source (PANalytical, Philips PW 1830, The Netherlands) with CuKα radiation at 40 kV and 40 mA. Diffraction spectra data were collected over the 2θ range of 1–30° with an acquisition time of 1 sat each step of 0.02°.

2.11. In vitro *release assay*

Dissolution studies of the CBZ released from nanoparticles were performed in a rotating paddle apparatus [47] (Vision Classic 6, Hanson Research, Chatsworth, CA, USA) at 100 rpm using 500 ml of KH_2PO_4 buffer (pH = 6.8) as dissolution media, filtered and deaerated with a 0.45-μm nylon filter before use. Bath temperature was set at 37.0 ± 0.5 °C.

Five millilitres of each formulation were placed in a prehydrated dialysis membrane (MWCO 10 kDa) and submerged in a vessel. A solution of free CBZ (without nanoparticles) of the same concentration was used as control. Samples were taken during 24 h at regular intervals of time, and immediately centrifuged at 3500 rpm. The amount released was determined spectrophotometrically at 285 nm (Helios Beta spectrophotometer, Thermo Fisher Scientific, Waltham, MA, USA). Trials were performed in triplicate, and the mean values were used for data analysis.

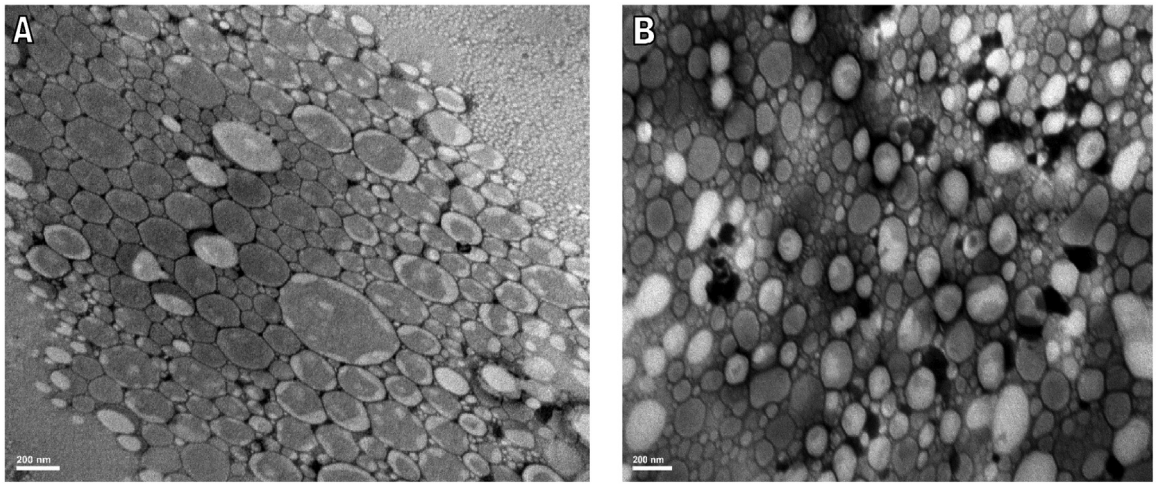

Fig. 1. TEM images of SLN-CBZ (A) and NLC-CBZ (B).

2.12. In vitro *cell permeability studies*

Parentand MDR1 transfected Madin–Darby canine kidney (MDCK) epithelial cells were obtained from the Netherlands Cancer Institute (Amsterdam, The Netherlands). Along with Caco-2 cells, MDCK cells are the most extensively used cells to assess drug permeability *in vitro*. Under standard culture conditions, MDCK cells develop tight junctions and form monolayers of polarized cells [48]. Here, MDCK-MDR1 cells were selected, which express human P-gp, so that the observed apparent permeability coefficients (Papp) also reflect the possible contribution of P-gp to drug transport across the epithelial cells [49,50].

Cells were grown in 25 cm^2 culture flasks using DMEM with 10% fetal bovine serum, 1% L-glutamine, 1% non-essential amino acids and penicillin and streptomycin at 37 °C in 5% CO_2 atmosphere. Cells were split twice a week at 70–80% confluence in a ratio of 1:20 or 1:30 using s Trypsin-EDTA solution (0.25%). All transport assays were done with cells from passages 19–43. Cells were kept at 37 °C in 5% CO_2.

The cells were seeded in 6-well Costar Snapwell plates with polycarbonate membrane inserts at a density of 50,000 cells per insert (1.12 cm^2) and grown for 4 days in culture medium. The medium was replaced every day. The apical media volume was 0.5 ml, and the basal volume was 2 ml. Integrity of the cell monolayers was determined by measuring the trans-epithelial electrical resistance (TEER, Ω cm^2) using an epithelial voltammeter (Millicell-ERS; Millipore Corporation).

On the day of the experiment, culture medium was removed, and cells were washed three times with media transport (HBSS, Hanks' balance salt solution, pH 7.4, Gibco-BRL). The filter inserts containing the cell monolayers were placed in a Using chamber, and were maintained at 37 °C under constant gassing with carbogen. Tested formulations were SLN, SLN-DMSO, NLC and NLC-DMSO, (DL=1.25%) prepared in transport media to a final concentration of 1.0 mM. Formulations were added to the apical chamber (4.0 ml). At 20, 40, 60, 80, 100 and 120 m, samples (400 μl) were taken from basolateral compartment followed by addition of 400 μl of transport media. A solution of free CBZ of the same concentration was used as control. Apparent permeability (Papp) was calculated with the equation:

$$P_{app} = \frac{1}{A \cdot C_0} x \left(dQ/dt\right) \quad (4)$$

where A is membrane surface area (1.12 cm^2), C_0 is the initial concentration in the donor compartment at t = 0, and dQ/dt is amount of drug transported within a given period of time.

2.13. *Stability studies*

Stability studies of all formulations were performed under storage conditions. Samples were kept at 2–8 °C. For these studies, individual vials for each replicate and time were used. Immediately after synthesis and every 30 days of storage for 90 days, CBZ content, particle size, PI and zeta potential were evaluated using the procedures described in the above sections.

2.14. *Anticonvulsant activity*

Pharmacological tests followed the standard procedures provided by the Antiepileptic Drug Development (ADD) Program of the National Institute of Neurological and Communicative Disorders and Stroke [51]. Swiss albino mice weighing between 18 and 25 g at time of testing were provided by the College of Veterinary of the National University of La Plata. Mice were housed in colony cages with a maximum of 10 mice per cage, with controlled room temperature at 20–22 °C. Cycles of 12 h light/dark were established, and *ad libitum* food and water provided. Mice adaptation to new environment was carried out for 5 days. Each day, 0.1 ml of physiological solution (PS) was administered intraperitoneally (*ip*) to every mouse.

Maximal electroshock seizures (MES) were elicited in mice by delivering a 60 Hz/50 mA electrical stimulus for 0.2 s via ear clip electrodes using the Ugo Basile electro-convulsive device. High conductivity gel was applied on each electrode to ensure an adequate electrical contact. In these conditions, maximal seizures are produced in virtually all normal mice. Maximal seizures typically consist in a short period of tonic flexion followed by a longer period of tonic extension of the hind limbs and a final clonic episode. It is considered as endpoint, for anticonvulsant protection, the inhibition of tonic hind limbs extension beyond a 90° angle to the torso.

One positive control (CBZ solution 30 mg/kg), two negative controls (PS and unloaded NLC-DMSO) and nanoparticle suspension (NLC DMSO, 30 mg/kg) were injected. Anticonvulsant activity was tested at 0.25, 0.5, 1.0, 2.0 and 4.0 h. A maximal volume of 10 ml/kg of freshly made solutions was *ip* administered.

RotoRod test was used to determine possible neurotoxic effects of formulation in test. A normal mouse can maintain its equilibrium on a rotating rod (6 rpm) for long periods of time. Failure to main-

Table 1
Composition and encapsulation efficiency (EE, %) of different SLN and NLC formulation containing CBZ in solid state or dissolved in 50 μl of DMSO, obtained by melt-emulsification/ultrasonication technique (MM: myristyl myristate, SS: cetyl esters wax). DL: theoretical drug load; EE: entrapment efficiency.

Samples	Lipid Phase			DL (%)	EE (%)*
	Lipid (g)	Oil (μl)	CBZ (mg)		
SLN_{MM}-CBZ	0.4	–	5	1.25	68.4
NLC_{MM}-CBZ	0.4	12	5	1.25	79.2
SLN_{MM}-CBZ (DMSO)	0.4	–	5	1.25	87.3
NLC_{MM}-CBZ (DMSO)	0.4	12	5	1.25	66.8
SLN_{SS}-CBZ	0.4	–	5	1.25	95.3 (0.6)^{d}
SLN_{SS}-CBZ	0.4	–	25	6.25	89.3 (3.2)^{a}
SLN_{SS}-CBZ (DMSO)	0.4	–	5	1.25	95.6 (0.4)^{d}
SLN_{SS}-CBZ (DMSO)	0.4	–	15	3.75	91.1 (1.1)^{abc}
SLN_{SS}-CBZ (DMSO)	0.4	–	20	5.00	90.8 (2.1)^{ab}
NLC_{SS}-CBZ	0.4	12	5	1.25	94.8 (0.6)^{d}
NLC_{SS}-CBZ(DMSO)	0.4	12	5	1.25	94.7 (1.0)^{bcd}
NLC_{SS}-CBZ (DMSO)	0.4	12	25	6.25	96.5 (0.3)^{d}

* Mean (n = 3) and SD are presented. Means with common letter indicates no significant difference ($p > 0.05$, Tukey HSD test).

tain balance during 1 min is an indication of possible neurological deficit [51].

In vivo animal testing was performed according to the guidelines of the Institutional Committee on Care and Use of Experimental Animals (CICUAL, *Facultad de Ciencias Exactas, Universidad Nacional de* La Plata, Argentina).

2.15. Statistical analysis

Experiments were carried out with a minimum of 3 independent replicas. When a different number of replicas were used, the number is specified in the corresponding section. According to the number of groups to be compared, comparisons of the means were performed by Student *t*-test or by analysis of variance (ANOVA, followed by Tukey's HSD test or Dunnet test for comparison to the control). A significance level of 0.05 was used. Prior to every parametric analysis, the assumptions of normality and homogeneity of variance were checked.

3. Results and discussion

3.1. Synthesis and characterization of SLN and NLC

SLN and NLC were prepared with different types and amounts of lipids, changing the tensioactive/lipid ratio and the initial amount of CBZ (Table 1). In two formulations (SLN-CBZ DMSO and NLC-CBZ DMSO) CBZ was previously dissolved in a minimum volume of DMSO (0.25%,v/v, which is below the maximum allowable limit established by FDA) and later incorporated to lipid phase [52]. Cetyl esters (SS) wax as main lipid component showed higher EE, compared to myristyl myristate (MM) formulation (Table 1). For this reason, only formulations containing SS were considered for further testing. In every case, the addition of 3.0% (wt) of the oil to NLCs formulations improved the encapsulation significantly, while higher amount of CBZ in SLN and SLN/DMSO produced a decrease in the EE. Besides, the EE of CBZ in all formulated lipid carriers were higher compared to previous reports [43].

3.2. Physicochemical characterization by DLS, DSC, TGA and DRX analysis

DLS analysis was performed in order to determine the mean particle size of the formulations (Table 1S). Results showed no significant differences ($p > 0.05$) in the mean diameter among the selected formulations, which displayed a narrow size distribution around160 nm. The zeta potential of all formulations was between −2.4 and −6.3 mV, where lower values corresponded to NLC formulation. The low zeta potential values observed can be explained considering the stabilization with a non-ionic surfactant (Pluronic F68). The steric stabilization is playing a key role to avoid the agglomeration of nanoparticles in suspension. On the other hand, particle size was slightly dispersed, with PI values below the optimal maximal limit of 0.3 similar to previously reported [53,54].

Table 2
Thermal properties of CBZ, bulk cetyl palmitate, and nanoparticles [SLN, SLN-CBZ, SLN-CBZ (DMSO) and NLC-CBZ (DMSO)]: melting enthalpy (ΔH_m); melting temperature (T_m); and crystallinity index (CI, %).

Sample	T_m (°C)	ΔH_m (J g^{-1})	CI (%)
Cetyl palmitate	49.2	192.1	100.0
CBZ	190.0–192.0	108.0	100.0
SLN	42.9–48.3	102.3	22.3
SLN-CBZ	44.2–49.6	120.0	26.1
SLN-CBZ (DMSO)	44.5–49.7	105.2	22.9
NLC-CBZ (DMSO)	44.6–49.8	88.9	19.4

Thermal characterization of nanoparticles was performed by DSC and TGA analysis to establish changes in the crystalline degree of the components after drug encapsulation. Overlaid DSC curves corresponding to CBZ, SLN, SLN-CBZ, SLN-CBZ (DMSO) and NLC-CBZ (DMSO) are shown in Fig. S2. All formulations showed an endothermic peak in the range of 44–49 °C that could be attributed to the melting point of the solid lipids. CBZ DSC thermogram exhibited a characteristic endothermic peak around its melting point (192 °C). Since none of the formulations showed a peak at such temperature, CBZ could be considered to be molecularly dispersed within the lipid matrix or in an amorphous state which can be explained considering the dissolution of CBZ in the molten lipid during loading [44].

CI (%)was estimatedassuming a lipid concentration of 2%by Eq. (4). CI (%)values of lipid dispersionsdecreased compared to bulk cetyl palmitate value (Table 2). Thatresult could be attributed to the addition of both oil and DMSO, which generates a lower stiffness of the matrix array than the original material. In concordance, calculation of meting enthalpies showed lower values,which are suggestinglower ordered and rigid structures and consequently, lower energies to overcome the lattice forces [55].

As a complement, TGA was performed to visualize changes in the thermal properties ofthe nanoparticles due to the incorporation of CBZ (Fig. 2).Thermal decomposition of CBZ proceeded in two steps of mass loss, between 88 °C to 342 °Cin nitrogen atmosphere. The first mass loss (88.0%) occurred in a single thermal event in the range 188–284 °C and corresponds to the thermal decomposition of anhydrous CBZ. The second mass loss (11.80%) between 284 °C and 342 °C, can be attributed to the decomposition of residual carbonaceous materials [56].

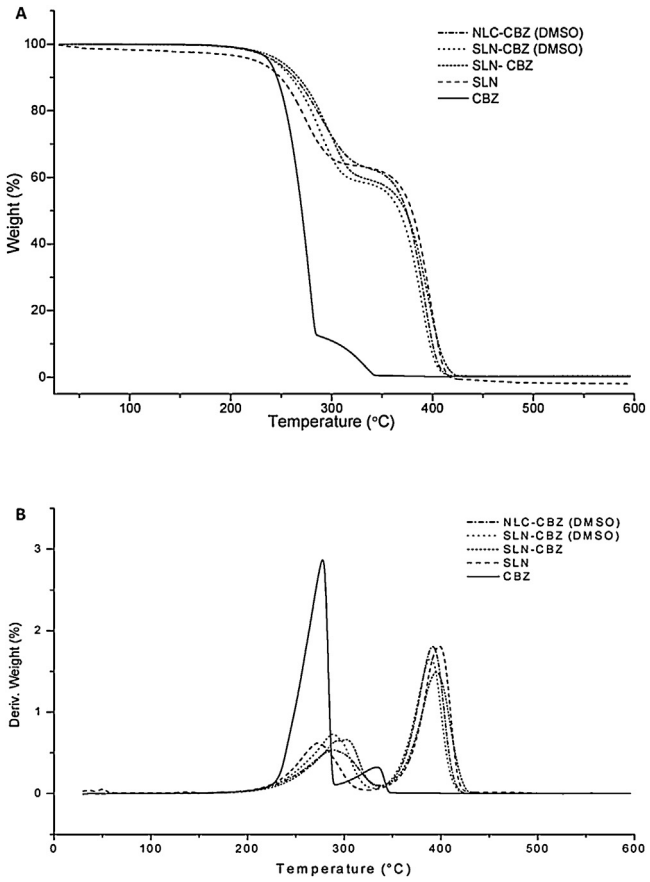

Fig. 2. Thermogravimetric curves (a) and derived thermogravimetric curves (b) of CBZ, SLN, SLN-CBZ, SLN-CBZ (DMSO) and NLC-CBZ.

On the other hand, SLN, SLN-CBZ, SLN-CBZ (DMSO) and NLC-CBZ (DMSO) showed biphasic thermal behaviour. The first thermal event occurred in the range of 190–337 °C with a weight loss of 35.2%, 40.7%, 41.5% and 37.4%, respectively. The second thermal event occurred between 337 and 425 °C with a weight loss of 65.1%, 58.9%, 58.2%, and 62.7%, respectively.None of the formulations showed significant differences in terms of their thermal behaviour compared to SLN without CBZ (SLN), and all of them maintained their stability at temperatures up to 180 °C. Those results are strongly suggesting the efficient encapsulation of CBZ in an amorphous state, which is an interesting point to allow its complete release in the physiological media.

Finally, to corroborate the previous observations, the X-ray diffraction patterns of CBZ, SLN, SLN-CBZ, SLN-CBZ (DMSO) and NLC-CBZ (DMSO) were analysed to get more insights of SLN structure (Fig. 3). CBZ pattern exposed multiple characteristic peaks at 2θ corresponding to 12.36°, 13.20°, 14.00° and 20.00°. However, those peaks were not observed in the XRD patterns of nanoparticles formulation, confirming that CBZ would be distributed in an amorphous state within the lipid matrix or molecularly dispersed in this one, in agreement with the previous results obtained in thermal analysis. On the other side, patterns corresponding to nanoparticles formulations exhibited peaks correlative to cetyl esters wax (19.18°, 21.44° and 23.25°) and confirm the solid crystalline structure of SLNs. Different polymorphisms of the lipid matrix were observed after preparation. Combination of β motifs (the most stable) and βí (a metastable form) of the lipids were displayed at 19.18° and 21.44° respectively, indicating the presence of partially disordered regions but maintaining a certain degree of crystallinity [57].

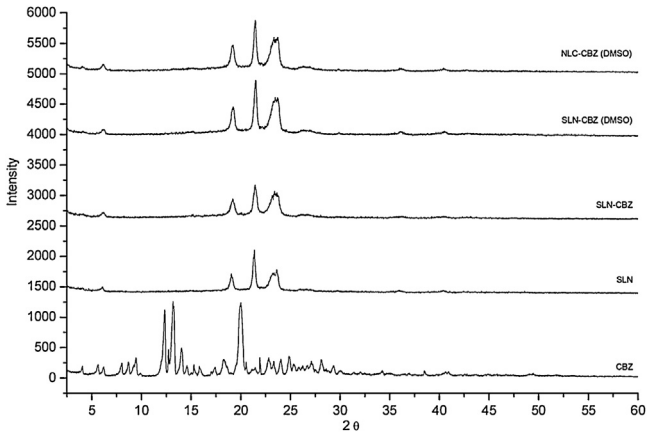

Fig. 3. XRD patterns of CBZ, SLN, SLN-CBZ, SLN-CBZ (DMSO) and NLC-CBZ (DMSO).

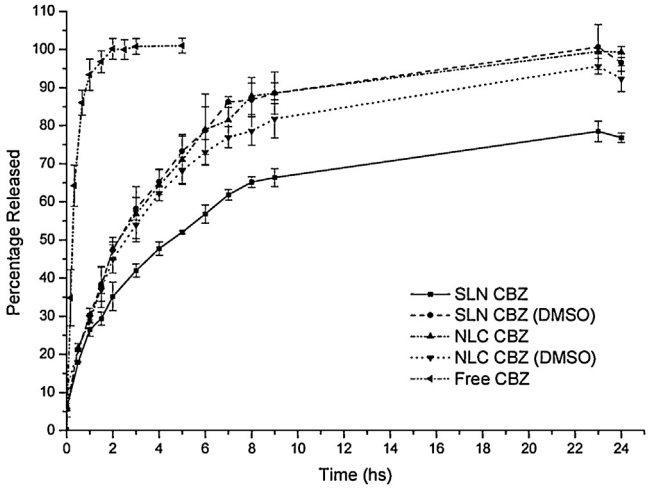

Fig. 4. Release profiles of SLN-CBZ, SLN-CBZ (DMSO), NLC-CBZ, NLC-CBZ (DMSO) and free CBZ.
Note: The experimental points represent the mean and SD values of n = 3.

3.3. *TEM and AFM analysis*

Size and morphological structure were further evaluated by different microscopy techniques. Images obtained by TEM (Fig. 1) showed spherical particles with a narrow particle size distribution. Image analysis using ImageJ software showed a mean particle size of 162 ± 27 nm for Fig. 1A and 140 ± 26 nm for Fig. 1B (N = 100 each). Furthermore, no morphological differences were observed among the developed formulations. These results are in accordance with the DLS analysis.

Those results were complemented by AFM analysis (Fig. S1). This technique was considered as a complementary morphologic characterization of the samples due to the fact that soft particles are likely flatten and broaden due to the occurrence of attractive forces with the support (as well as to the weak forces of the probe, even in tapping mode). Effectively, size analysis by AFM showed flattened particles, with heights ranging from 15 to 70 nm. However, the sizes observed in the xy plane were in the range of the diameters observed by TEM images (187 ±60 nm).

3.4. In vitro *release assay*

The *in vitro* release profiles of CBZ from nanoparticles are shown in Fig. 4. In comparison with free CBZ, all formulations showed a controlled release of CBZ during 24 h, with an initial burst release

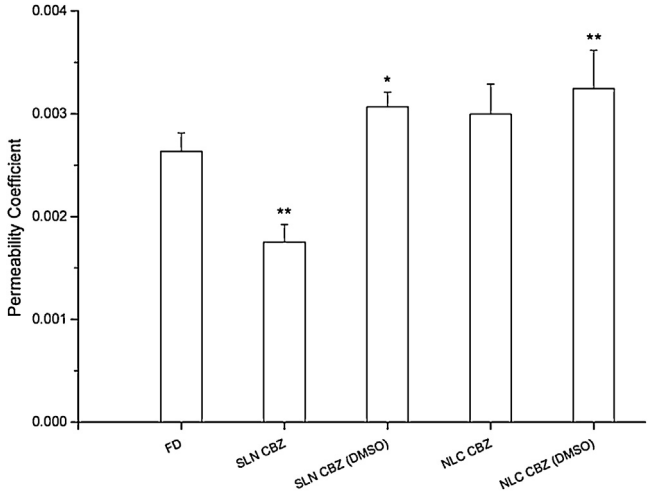

Fig. 5. Permeability coefficients of tested formulations.
Note: * and ** represents significant and very significant differences ($p < 0.05$ and $p < 0.01$, respectively, Dunnet test) in comparison with the control (free drug, FD). Results are shown the mean and SD of n = 5.

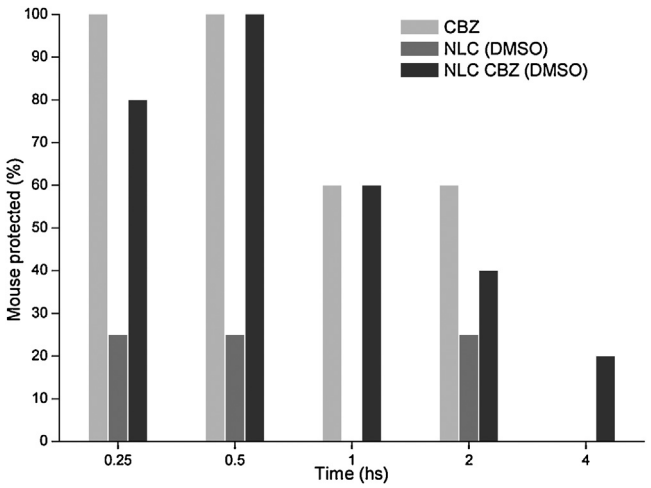

Fig. 6. In *vivo* evaluation of anticonvulsant activity represented by the percentage of mice protected at each time post-dose, for physiological solution (PS), vehicle [NLC (DMSO)], solution of CBZ and the formulation tested [NLC CBZ (DMSO)] at a dose of 30 mg/kg.

associated to free drug contained in the suspension and drug adsorbed at the nanoparticles surface [58]. The less pronounced release rate observed afterwards could be attributed to the diffusion of the drug from the lipid matrix to the media. A relatively higher release rate of SLN CBZ (DMSO), NLC-CBZ and NLC-CBZ (DMSO) (in comparison with SLN-CBZ) was observed and could be explained by the increased mobility of the drug dispersed in a more amorphous matrix (due to the incorporation of oil, DMSO or both), which results in a fast diffusion [33]. Nevertheless, the release kinetic achieved by the nanoparticles is in close agreement with the pharmacopoeial requirements for CBZ extended-release products (between 65 and 90% of the drug must dissolve in 12 hs, and not less than 75% in 24 hs) [47].

Release kinetic models of the developed nanosystems fitting the experimental points were evaluated. In all cases, the model developed by Baker and Lonsdale was the one that best fit to the data ($R^2 = 0.94$, 0.97, 0.97 and 0.97 for SLN-CBZ, SLN CBZ (DMSO), NLC-CBZ and NLC-CBZ (DMSO) respectively). The model describes controlled drug release from spherical shape matrices, with a combination of diffusion and degradation as factors responsible for the release mechanism and derived from Higuchi model [59,60].

3.5. In vitro *cell permeability studies*

The results of *in vitro* cell permeability studies are displayed in Fig. 5 as the mean and SD values of the permeability coefficient of all formulations (n = 5). Wells with a CBZ solution in Hank's buffer were evaluated as controls. The Dunnet test was applied to compare the mean values with a control (free drug). Formulations SLN DMSO and NLC DMSO showed significantly enhanced permeability respect to free drug with a confidence of 95% and 99%, respectively. In contrast, SLN without DMSO displayed a reduced permeability coefficient in comparison with free drug. Although all formulations possessed similar entrapment efficiency, particle size distribution and zeta potential, formulations containing a liquid lipid (nanostructured) and DMSO could modify lipid matrix making it more deformable and allowing nanoparticles to across the cell monolayer more easily, leading to an increase of CBZ permeation. Neves et al. have demonstrated that TEER values in the presence of NLC were decreased in 10% regarding the presence of fresh medium. This effect could indicate a partial opening of tight junctions between epithelial cells [61].

3.6. *Stability studies*

All SLN and NLC formulations were stored at 2–8 °C for 90 days and no significant changes ($p > 0.05$) in CBZ content (%), particle size, zeta potential and PI were found along the tested period, suggesting that nanoparticles are stable under the storage conditions (Fig. S3).

3.7. *Anticonvulsant activity*

The results of the anticonvulsant assays in mice models are shown in Fig. 6. Negative control (PS) did not present anticonvulsant activity, while the vehicle control displayed protection in at least one animal in almost all times. On the other hand, positive control (free drug: FD) presented activity in almost all animals at each time except at 4 h, where no anticonvulsant activity was observed. Similarly, nanoparticle formulations showed anticonvulsant activity like the free drug. The NLC showed protection against seizures in 1 out of 5 mice (20%) at 4 h, whereas no protection was observed with the free drug. This preliminary result are in agreement with recent reports [62,63] that suggest an enhanced duration of the therapeutic effects of drugs encapsulated into lipid nanoparticles. Taking advantage of the fact that these nanosystems have a lower intrinsic toxicity and that they deliver the drug in a prolonged manner, further evaluation at higher doses and prolonged times will be performed to study this possible advantage of the NLC system over the free drug. On the other hand, all tested formulations did not show neurotoxic effects in any tested animal evaluated by the RotoRod test.

In addition, the feasibility of these NLC to increase the anticonvulsant activity of the drug could be further explored by other administrations routes, and particularly intranasal delivery as was proposed by other recent works for brain targeting [64,65].

4. Conclusion

The CBZ-SLN and CBZ-NLC presented in this work are original in terms of their technology, since they comprise only lipid components, they are prepared by the melt-emulsification technique and achieve high drug loading capacity even without the use of organic solvents. On the other hand, these novel formulations possess several advantages over the only previously reported nanolipid system [43], such as optimum particle size to avoid their removal by the mononuclear phagocyte system [54] (*ca.*160 nm), with low PI

(lower than 0.3) and high encapsulation efficiency (higher than 85% for all the selected formulations). Moreover, formulations proved to be stable in terms of their EE, particle size, zeta potential and PI at 4 °C for 90 days.

In addition, thermal and crystallographic experiments suggested that CBZ was incorporated into the lipid matrix in amorphous state which facilitates the dissolution of the drug in physiological simulated medium. As an additional feature, the systems exhibited a sustained CBZ release profile, determined under biopharmaceutically relevant conditions for at least 24 h, fitting a model that describes the drug release from a spherical matrix. Some of the prepared systems also achieved an enhanced CBZ permeability through MDCK cell monolayer. Finally, our CBZ-loaded nanolipid systems have shown a comparable protective effect to free CBZ in the MES seizure model.

The developed system represents a novel and interesting approach to improve the bioavailability of AEDs and overcome some of the challenges commonly found in the treatment of CNS conditions.

Conflict of interest

The authors confirm that this article content has no conflicts of interest.

Acknowledgements

The authors would like to thank UNLP and CONICET. The present work was supported by Argentine grants from CONICET (National Council for Science and Technology, PIP 0498), The National Agency of Scientific and Technological Promotion (ANPCyT, PICT 2011-2116, PICT 2013.3175), UNLP (National University of La Plata, 11/X545 and PRH 5.2) to GRC. Authors want to thank Dr. E.D. Prieto for AFM technical support and analysis (INIFTA) and CRODA Argentina for kindly donating the lipids.

Appendix A. Supplementary data

Supplementary data associated with this article can be found, in the online version, at https://doi.org/10.1016/j.colsurfb.2018.03.052.

References

[1] M.L. Etheridge, et al., The big picture on nanomedicine: the state of investigational and approved nanomedicine products, Nanomedicine 9 (2013) 1–14.
[2] B.A. Grzybowski, W.T.S. Huck, The nanotechnology of life-inspired systems, Nat. Nanotechnol. 11 (2016) 585–592.
[3] F. Araújo, et al., Safety and toxicity concerns of orally delivered nanoparticles as drug carriers, Expert Opin. Drug Metab. Toxicol. 11 (2015) 381–393.
[4] P. Vlieghe, M. Khrestchatisky, Medicinal chemistry based approaches and nanotechnology-based systems to improve CNS drug targeting and delivery, Med. Res. Rev. 33 (2013) 457–516.
[5] A.M. Cardoso, et al., Recent trends in nanotechnology toward CNS diseases, Int. Rev. Neurobiol. (2016) 1–40.
[6] A. Mahringer, et al., The ABC of the blood-brain barrier – regulation of drug efflux pumps, Curr. Pharm. Des. 17 (2011) 2762–2770.
[7] R.S. Fisher, et al., ILAE official report: a practical clinical definition of epilepsy, Epilepsia 55 (2014) 475–482.
[8] WHO, Epilepsy Fact Sheet Nº 999, 2017, Available at www.who.int/mediacentre/factsheets/fs999/en/ (Accessed 09/18/2017).
[9] I.A. Lie, et al., Treatment non-adherence as a trigger for status epilepticus: an observational retrospective study based on therapeutic drug monitoring, Epilepsy Res. 113 (2015) 28–33.
[10] C.M.M. Ferrari, et al., Factors associated with treatment non-adherence in patients with epilepsy in Brazil, Seizure 22 (2013) 384–389.
[11] S. Wiebe, N. Jette, Pharmacoresistance and the role of surgery in difficult to treat epilepsy, Nat. Rev. Neurol. 8 (2012) 669–677.
[12] W. Löscher, et al., New avenues for anti-epileptic drug discovery and development, Nat. Rev. Drug Discov. 12 (2013) 757–776.
[13] A. Talevi, Computational approaches for innovative antiepileptic drug discovery, Expert Opin. Drug Discov. 11 (2016) 1001–1016.
[14] M. Mula, Third generation antiepileptic drug monotherapies in adults with epilepsy, Expert Rev. Neurother. 16 (2016) 1087–1092.
[15] K. Radhakrishnan, Challenges in the management of epilepsy in resource-poor countries, Nat. Rev. Neurol. 5 (2009) 323–330.
[16] M. Fresta, et al., Preparation and characterization of polyethyl-2-cyanoacrylate nanocapsules containing antiepileptic drugs, Biomaterials 17 (1996) 751–758.
[17] J. Darius, et al., Influence of nanoparticles on the brain-to-serum distribution and the metabolism of valproic acid in mice, J. Pharm. Pharmacol. 52 (2000) 1043–1047.
[18] Z. Fang, et al., Pluronic P85-coated poly(butylcyanoacrylate) nanoparticles overcome phenytoin resistance in P-glycoprotein overexpressing rats with lithium-pilocarpine-induced chronic temporal lobe epilepsy, Biomaterials 97 (2016) 110–121.
[19] D. Sakthivel, G. Arunachalam, Preparation and characterization of polymeric nanoparticles used in the treatment of epilepsy, J. Pharm. Sci. & Res. 9 (2017) 298–301.
[20] A. Lopalco, et al., Oxcarbazepine-loaded polymeric nanoparticles: development and permeability studies across in vitro models of the blood-brain barrier and human placental trophoblast, Int. J. Nanomed. 10 (2015) 1985–1996.
[21] D. Dickens, et al., A multi-system approach assessing the interaction of anticonvulsants with P-gp, PLoS One 8 (2013) e64854.
[22] Y. Liu, et al., More accurate matrix-matched quantification using standard superposition method for herbal medicines, J. Chromatogr. A 1254 (2012) 43–50.
[23] M.E. Ali, A. Lamprecht, Polyethylene glycol as an alternative polymer solvent for nanoparticle preparation, Int. J. Pharm. 456 (2013) 135–142.
[24] M. Hamidi, et al., Valproate-loaded hydrogel nanoparticles: preparation and characterization, J. Appl. Polym. Sci. 124 (2012) 4686–4693.
[25] M.-H. Hsiao, et al., Design and characterization of a novel amphiphilic chitosan nanocapsule-based thermo-gelling biogel with sustained in vivo release of the hydrophilic anti-epilepsy drug ethosuximide, J. Control Release 161 (2012) 942–948.
[26] B. Wilson, et al., Albumin nanoparticles for the delivery of gabapentin: preparation, characterization and pharmacodynamic studies, Int. J. Pharm. 473 (2014) 73–79.
[27] G. Vignaroli, et al., Improvement of pyrazolo[3,4-d]pyrimidines pharmacokinetic properties: nanosystem approaches for drug delivery, Sci. Rep. 6 (2016) 21509.
[28] L. Jiang, et al., A nontoxic disulfide bond reducing method for lipophilic drug-loaded albumin nanoparticle preparation: formation dynamics, influencing factors and formation mechanisms investigation, Int. J. Pharm. 443 (2013) 80–86.
[29] K. Langer, et al., Human serum albumin (HSA) nanoparticles: reproducibility of preparation process and kinetics of enzymatic degradation, Int. J. Pharm. 347 (2008) 109–117.
[30] M.A. Vandelli, et al., Gelatin microspheres crosslinked with D,L-glyceraldehyde as a potential drug delivery system: preparation, characterisation, in vitro and in vivo studies, Int. J. Pharm. 215 (2001) 175–184.
[31] C. Tapeinos, et al., Advances in the design of solid lipid nanoparticles and nanostructured lipid carriers for targeting brain diseases, J. Control Release 264 (2017) 306–332.
[32] G. Graverini, et al., Solid lipid nanoparticles for delivery of andrographolide across the blood-brain barrier: in vitro and in vivo evaluation, Coll. Surf. B Biointerfaces 161 (2018) 302–313.
[33] M.E. Ruiz, et al., Applications of nanosystems to anticancer drug therapy (Part II. Dendrimers micelles, lipid-based nanosystems), Recent Pat. Anticancer Drug Discov. 9 (2014) 99–128.
[34] N. Gandomi, et al., Solid lipid nanoparticles surface modified with anti-contactin-2 or anti-neurofascin for brain-targeted delivery of medicines, Pharm. Dev. Technol. 22 (2017) 426–435.
[35] R. Dal Magro, et al., ApoE-modified solid lipid nanoparticles: a feasible strategy to cross the blood-brain barrier, J. Control Release 249 (2017) 103–110.
[36] G. Abdelbary, R.H. Fahmy, Diazepam-loaded solid lipid nanoparticles: design and characterization, AAPS PharmSciTech. 10 (2009) 211–219.
[37] J. Varshosaz, et al., Production and optimization of valproic acid nanostructured lipid carriers by the Taguchi design, Pharm. Dev. Technol. 15 (2010) 89–96.
[38] G. Leyva-Gómez, et al., Nanoparticle formulation improves the anticonvulsant effect of clonazepam on the pentylenetetrazole-Induced seizures: behavior and electroencephalogram, J. Pharm. Sci. 103 (2014) 2509–2519.
[39] A. Loureiro, et al., Albumin-based nanodevices as drug carriers, Curr. Pharm. Des. 22 (2016) 1371–1390.
[40] M. Bankstahl, et al., Knockout of P-glycoprotein does not alter antiepileptic drug efficacy in the intrahippocampal kainate model of mesial temporal lobe epilepsy in mice, Neuropharmacology 109 (2016) 183–195.
[41] J.J. Poza-Aldea, A proposal for a model to replace carbamazepine or oxcarbazepine by eslicarbazepine acetate in clinical practice, Rev. Neurol. 63 (2016) 219–223.

[42] C. Zhang, et al., In vitro transport profile of carbamazepine, oxcarbazepine, eslicarbazepine acetate, and their active metabolites by human P-glycoprotein, Epilepsia 52 (2011) 1894–1904.
[43] R. Nair, et al., Formulation and evaluation of chitosan solid lipid nanoparticles of carbamazepine, Lipids Health Dis. 11 (2012) 72.
[44] G.A. Islan, et al., Smart lipid nanoparticles containing levofloxacin and DNase for lung delivery. Design and characterization, Coll. Surf. B Biointerfaces 143 (2016) 168–176.
[45] B. Rodenak-Kladniew, et al., Design, characterization and in vitro evaluation of linalool-loaded solid lipid nanoparticles as potent tool in cancer therapy, Coll. Surf. B Biointerfaces 154 (2017) 123–132.
[46] V. Makwana, et al., Solid lipid nanoparticles (SLN) of Efavirenz as lymph targeting drug delivery system: elucidation of mechanism of uptake using chylomicron flow blocking approach, Int. J. Pharm. 495 (2015) 439–446.
[47] The United States Pharmacopeia 34, United States Pharmacopeia Convention, Rockville, MD, 2011.
[48] D.A. Volpe, Drug-permeability and transporter assays in Caco-2 and MDCK cell lines, Future Med. Chem. 3 (2011) 2063–2077.
[49] A. Talevi, L.E. Bruno-Blanch, Efflux-transporters at the blood-brain barrier: therapeutic opportunities, in: P.A. Montenegro, S.M. Juárez (Eds.), Blood-Brain Barrier New Res., 1 st ed., Nova Publishers, New York, 2012, pp. 117–144.
[50] H. Glavinas, et al., The role of ABC transporters in drug resistance, metabolism and toxicity, Curr. Drug Deliv. 1 (2004) 27–42.
[51] J.P. Stables, H.J. Kupferberg, The NIH Anticonvulsant Drug Development (ADD) Program: preclinical anticonvulsant screening project, Available at Www.ninds.nih.gov/research/asp/addadd_review.pdf (Accessed 09/23/2017).
[52] FDA, Guidances, Appendix 6. Toxicological Data For Class 3 Solvents, Available at www.fda.gov/downloads/drugs/guidancecomplianceregulatoryinformation/guidances/ucm073403.pdf (Accessed 09/25/2017).
[53] W. Schärlt, Light Scattering from Polymer Solutions and Nanoparticle Dispersions, Springer-Verlag, Berlin, 2007.
[54] S. Das, A. Chaudhury, Recent advances in lipid nanoparticle formulations with solid matrix for oral drug delivery, AAPS PharmSciTech. 12 (2011) 62–76.
[55] P.V. Pople, K.K. Singh, Development and evaluation of topical formulation containing solid lipid nanoparticles of vitamin A, AAPS PharmSciTech. 7 (2006) E63–E69.
[56] M. Aparecida, et al., Thermoanalytical studies of carbamazepine: hydration/dehydration, thermal decomposition, and solid phase transitions, Braz. J. Pharm. Sci. 50 (2014).
[57] Y. Rosiaux, et al., Solid lipid excipients as matrix agents for sustained drug delivery, in: Excip. Appl. Formul. Des. Drug Deliv., Springer International Publishing, Cham, 2015, pp. 237–271.
[58] M.S. Baig, et al., Application of Box-Behnken design for preparation of levofloxacin-loaded stearic acid solid lipid nanoparticles for ocular delivery: optimization, in vitro release, ocular tolerance, and antibacterial activity, Int. J. Biol. Macromol. 85 (2016) 258–270.
[59] R.W. Baker, Controlled Release of Biologically Active Agents, Wiley-Interscience, New York, 1987.
[60] K. Shi, et al., Tocopheryl succinate-based lipid nanospheres for paclitaxel delivery: preparation, characters, and in vitro release kinetics, Drug Deliv. 17 (2010) 1–10.
[61] A.R. Neves, et al., Nanoscale delivery of resveratrol towards enhancement of supplements and nutraceuticals, Nutrients 8 (2016) 131.
[62] E. Joseph, et al., Design and in vivo evaluation of solid lipid nanoparticulate systems of Olanzapine for acute phase schizophrenia treatment: investigations on antipsychotic potential and adverse effects, Eur. J. Pharm. Sci. 104 (2017) 315–325.
[63] M. Cirri, et al., Development and in vivo evaluation of an innovative hydrochlorothiazide-in cyclodextrins-in solid lipid nanoparticles formulation with sustained release and enhanced oral bioavailability for potential hypertension treatment in pediatrics, Int. J. Pharm. 521 (2017) 73–83.
[64] G. Rassu, et al., Nose-to-brain delivery of BACE1 siRNA loaded in solid lipid nanoparticles for Alzheimer's therapy, Coll. Surf. B Biointerfaces 152 (2017) 296–301.
[65] A.M. Fatouh, et al., Intranasal agomelatine solid lipid nanoparticles to enhance brain delivery: formulation, optimization and in vivo pharmacokinetics, Drug Des. Dev. Ther. 11 (2017) 1815–1825.